J Mater Sci (2008) 43:6651–6660
DOI 10.1007/s10853-008-2691-1

Modeling of evolving damage in high temperature polymer matrix composites subjected to thermal oxidation

Samit Roy · Sushil Singh · Gregory A. Schoeppner

Received: 4 April 2008 / Accepted: 30 April 2008 / Published online: 9 August 2008

Abstract This paper describes mechanism-based modeling of damage evolution in high temperature polymer matrix composites (HTPMC) under thermo-oxidative aging conditions. Specifically, a multi-scale model based on micro-mechanics analysis in conjunction with continuum damage mechanics (CDM) is developed to simulate the accelerated fiber–matrix debond growth in the longitudinal direction of a unidirectional HTPMC. Using this approach, one can relate the behavior of composites at the micro-level (representative volume element) to the macro-level (structural element) in a computationally tractable manner. Thermo-oxidative aging is simulated with diffusion-reaction model in which temperature, oxygen concentration, and weight loss effects are considered. For debond growth simulation, a model based on Darcy's laws for oxygen permeation in the fiber–matrix interface is employed, that, when coupled with polymer shrinkage, provides a mechanism for permeation-controlled debond growth in HTPMC. Benchmark of model prediction with experimental observations of oxidation layer growth is presented, together with a laminate thermo-oxidative life prediction model based on CDM to demonstrate proof-of-concept.

S. Roy (✉) · S. Singh
Department of Aerospace Engineering and Mechanics, University of Alabama, Tuscaloosa, AL 35487-0280, USA
e-mail: sroy@eng.ua.edu

G. A. Schoeppner
Air Force Research Laboratory (AFRL), Materials and Manufacturing Directorate, Structural Materials Branch (MLBC), Wright-Patterson AFB, Dayton, OH 45433-7750, USA

Introduction

In order to support materials selection for the next-generation supersonic transport aircraft, a study has been undertaken to evaluate the material constitutive relationships needed to describe advanced polymer matrix composites under conditions of high load and elevated temperature. The primary challenge to the use of HTPMC is due to hygro-thermal effects at temperature (100–300 °C) resulting in thermo-oxidative degradation and accelerated damage evolution. Various researchers have studied the thermo-oxidative aging process by developing model based design and novel-material systems that enhance the life and affordability of HTPMC. Colin et al. [1] developed a kinetic model to predict the depth of the oxidized layer for a F655-2 bismaleimide polymer resin. The model is based on a differential equation analogous to Fick's law in which the oxygen diffusion and its consumption rate $r(C)$ are coupled, where C is the oxygen concentration. The mathematical form of the consumption term, $r(C)$, is derived from the mechanistic scheme of branched radical chain oxidation. Their model predictions were in excellent agreement with experimental results. More recently, Colin et al. [2] enhanced their kinetic model to predict relative mass loss in a T800H/BMI composite by assuming that the volatile formation results essentially from hydroperoxide decomposition. The enhanced model was also able to take into account the fact that mass loss is reduced due to the stabilizing effect of carbon fibers due to the scavenging of the peroxyl radicals by carbon. Again, excellent agreement with experimental gravimetric results was observed. Tandon et al. [3, 4] extended the kinetic model by introducing the concept of polymer availability state variable, thereby producing predictive oxidative layer growth simulations for a high temperature polyimide,

PMR-15. Macroscopic weight loss measurements were used to determine the reaction and polymer consumption parameters. A parametric sensitivity analysis was used to determine the sensitivity of the controlling parameters. It was observed that the oxidation growth process was diffusion controlled, and that the diffusivity of the oxidized zone is the controlling parameter. Recently, Pochiraju et al. [5] have studied the thermo-oxidative behavior of unidirectional composite material. Their work deals with thermo-oxidative layer growth and damage growth with time. The modulus of PMR-15 is sensitive to the temperature and oxidation state. Due to strong anisotropy in thermo-oxidative response of G30-500/PMR-15 composite, accelerated oxide layer growth is observed in the fiber direction as compared with the direction transverse to the fibers. Homogenization techniques are used to determine the effective diffusivity of the composite lamina. They have demonstrated the effect of fiber fraction on diffusivity and the effect of a diffusive interface at the lamina scale. It is also observed that compressive modulus of PMR-15 resin decreases from 4.72 to 3.39 GPa due to temperature rise from 25 to 288 °C as obtained from nano-indentation data of un-oxidized resin. Wang and Chen [6] have developed a computational micromechanics approach, based on a recently developed coupled constitutive theory with reaction and micro-structural damage for polymer–matrix composites in a high-temperature environment. Micromechanics formulation of the problem is derived to include coupled anisotropic thermal oxidation reaction, mass transport, and thermo-mechanical damage in the fiber composites. Numerical solutions are developed for the thermal oxidation problem of a carbon/polyimide composite at elevated temperatures subject to thermo-mechanical loading. Talreja [7] has developed constitutive stress–strain relationships for basic configurations containing distributed damage entities. In this model, a continuum concept is used which considers composites as homogeneous anisotropic bodies with distributed damage as the internal structure. It uses the basic laws of thermodynamics and damage tensor as internal variables in the functional relationships of response functions. Recently, Talreja [8] discussed multi-scale modeling aspects of damage and operating mechanisms in unidirectional ceramic matrix composites and cross-ply polymer matrix composite laminates. Two multi-scale modeling strategies—continuum damage mechanics (CDM) and synergistic damage mechanics—are proposed in the context of deformational response. These are homogenization techniques where material micro-structure and micro-damage structure are treated as smeared tensor fields. A set of response functions are expressed in terms of field variables, which represent the smeared-out fields of evolving damage entities.

The proposed approach in this paper focuses on transitioning the micro-mechanics based kinetic models as discussed earlier, to the macro-scale structural level, through the use of CDM. The strong anisotropy observed in the thermal-oxidation of unidirectional composite lamina is accounted for in this model. Darcy's law is employed to model oxygen permeation in the porous region at the fiber/matrix interface to develop a shrinkage induced, permeation-controlled debond growth model. Debond initiation and growth are incorporated in the model through the use of a cohesive layer with a prescribed traction-separation law, and the damage parameters thus obtained are used to predict long-term behavior at the laminate level.

Mathematical formulation of thermo-oxidation model

Modified Fick's Law for diffusion and polymer consumption

Modified Fick's Law for diffusion reaction with orthotropic diffusivity is given by Crank [9],

$$\frac{\partial C}{\partial t} = \left(D_{11}\frac{\partial^2 C}{\partial x^2} + D_{22}\frac{\partial^2 C}{\partial y^2} + D_{33}\frac{\partial^2 C}{\partial z^2} \right) - r(C) \tag{1}$$

with $C(x,y,z,t)$ denoting the oxygen concentration field at any time within a polymer with orthotropic diffusivities D_{ij}, and a polymer consumption reaction rate given by $r(C)$.

Because three distinct zones—fully oxidized, active reaction, and unoxidized—are typically formed during polymer oxidation [3, 4], the diffusivity in the active zone is derived based on linear interpolation of the diffusivities in the oxidized and unoxidized regions. The interpolation is carried out using a polymer state variable, φ, such that $\varphi = 1$ when the polymer is unoxidized, and $\varphi = \phi_{ox}$ when the polymer is fully oxidized. The diffusivity in the active zone is then approximated using the interpolation,

$$D_{ij}(\phi) = D_{ij}^{un}\frac{\phi - \phi_{ox}}{1 - \phi_{ox}} + D_{ij}^{ox}\frac{1 - \phi}{1 - \phi_{ox}} \tag{2}$$

where D_{ij}^{un} is the diffusivity in the unoxidized zone and D_{ij}^{ox} is the diffusivity in the oxidized zone.

Polymer reaction rate $r(C)$

The polymer reaction rate is obtained using the mechanistic scheme of branch radical chain reaction developed in [1],

$$r(C) = R_0 f(C) \tag{3}$$

$$f(C) = \frac{2\beta C}{1 + \beta C}\left[1 - \frac{\beta C}{2(1 + \beta C)}\right] \tag{4}$$

where R_0 is a constant or a temperature dependent parameter and the reaction rate coefficient, β, is a material constant.

Evolution of polymer state variable ϕ

The evolution law for the polymer state variable is given as [3],

$$\frac{d\phi}{dt} = -\alpha r(C) \tag{5}$$

where α is a reaction rate constant. Assuming the initial condition that $\phi = 1$ at $t = 0$ (un-oxidized state) and integrating Eq. 5, gives

$$\phi(t) = \phi_0 - \int_0^t \alpha r(C)dt = 1 - \int_0^t \alpha r(C)dt \tag{6}$$

If it is assumed that ϕ_{ox} is the cut-off value of ϕ in the oxidized zone when all of the consumable portion of the polymer has been consumed, then $\phi(t) = \phi_{ox}$ in the fully oxidized zone.

Cohesive layer modeling of anisotropy in thermo-oxidative degradation

It has been observed in surface weight-loss rate experiments performed on unidirectional G30-500/PMR-15 polymer matrix composite laminate aged at 288 °C at Air Force Research Laboratory (AFRL), that oxygen diffusion, and consequently, polymer weight loss exhibits anisotropic behavior. The weight loss in the direction transverse to the fibers is actually lower than the weight-loss for neat resin samples due to the retarding effect of the carbon fibers on oxygen diffusion, as predicated by the rule-of-mixtures. However, the weight loss in the longitudinal (fiber) direction is observed to be greatly accelerated due to synergistic interactions between the fiber, matrix, and the interface. It is conjectured that polymer shrinkage due to thermal oxidation may be responsible for debond initiation and propagation along fiber–matrix interfaces, thereby allowing accelerated penetration of oxygen into the laminate, followed by thermal oxidation. A micrograph showing evidence of fiber/matrix debond due to thermo-oxidative resin shrinkage is presented in Fig. 1. To simulate this effect, a cohesive layer model was introduced at the interface of the polymer and fiber within the framework of a finite element analysis of a representative volume element (RVE) using an in-house test-bed code (NOVA-3D, [10, 11]). Based on a cohesive zone model proposed by Needleman [12], a cubic traction-separation law is employed to simulate the material behavior at the fiber/matrix interface, as shown in Fig. 2. In the present model, the cohesive layer is assumed to have a finite thickness, approximately equal to the thickness of the sizing at the fiber/matrix interface. Material properties of the fiber, matrix and cohesive layer are given in Table 1. It is

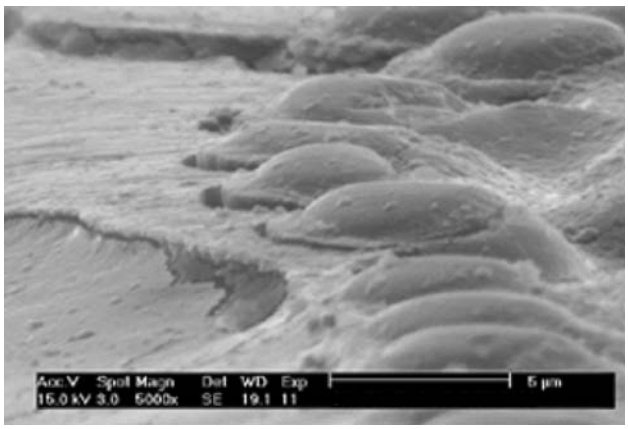

Fig. 1 Micrograph of fiber/matrix debond due to thermo-oxidation in G30-500/PMR-15 composite at 288 °C in air

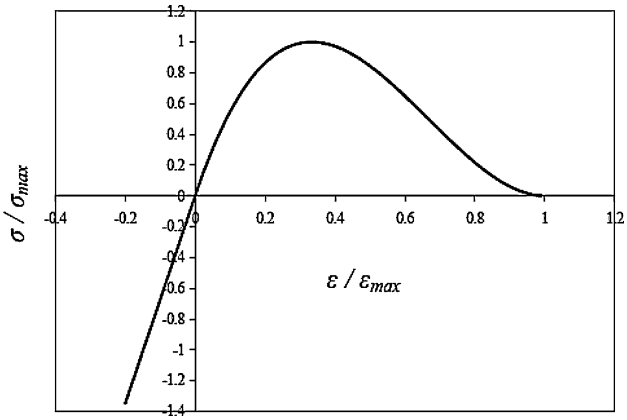

Fig. 2 Normalized cubic traction-separation law for cohesive layer

important to note that the elastic modulus of polymer matrix varies with aging time and polymer state variable φ as suggested by Wise et al. [13],

$$E(\phi,T,t) = E_{un}(T)\exp\left(K_{ox}\frac{1-\phi}{1-\phi_{ox}}\right)\exp\left(K_{nox}\frac{1-\phi}{1-\phi_{ox}}t\right) \tag{7}$$

where $K_{nox} = 0$ and $K_{ox} = 0.1878$ for PMR-15, T is temperature, and t is time. Further, it is notable that significant polymer shrinkage strains—on the order of 30–40% at elevated temperatures—were observed by researchers at the Air Force Research Laboratory (AFRL, Dayton, OH, USA).

Analytical model to predict debond length using Darcy's law for oxygen diffusion

Assuming that the fiber/matrix debond is initiated and propagated by the shrinkage strain in the surrounding polymer matrix due to oxidative degradation, it is proposed that the debond fracture surface is not smooth, but that it exhibits

Table 1 Material properties of G30-500 carbon fiber, polymer matrix (PMR-15), and cohesive layer

Material properties	Polymer matrix	Carbon fiber	Cohesive layer
Young's modulus (GPa) (un-oxidized)	2.6	240	–
Poisson's ratio	0.36	0.4	–
Maximum stress (MPa)	–	–	10
Maximum strain	–	–	0.1
D_{un} ($\times 10^{-12}$ m^2/min)	78.6	7.86	78.6
D_{ox} ($\times 10^{-12}$ m^2/min)	150	15.0	150
R_0 ($\times$ mol/m^3 min)	0.0583	–	0.0583
Threshold value of polymer state variable (φ_{ox})	0.18	–	0.18
Percent shrinkage strain	5%	–	5%
Reaction rate parameter (α)	0.2	–	0.2
β	0.919	–	0.919
λ(CTE) (/°C)	1.0×10^{-5}	–	1.0×10^{-5}
Fiber radius (R) in (m)	–	2.5×10^{-6}	–

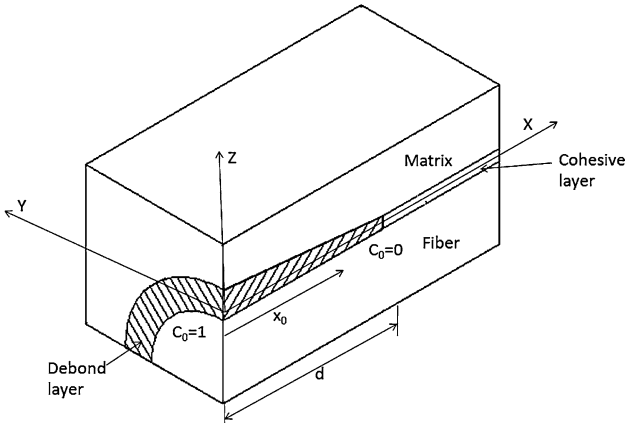

Fig. 3 Debonding due to oxygen permeation/diffusion at the interface of fiber and matrix

significant roughness due to the presence of oxidation products as well as fractured polymer fibrils along the interface. Consequently, the flow of oxygen to the debond tip may be represented as one-dimensional axisymmetric flow through a porous media, as depicted in Fig. 3, where d is the debond length, and x_0 is the length along which permeation of oxygen is occurring through the porous debond region. Assuming flow controlled debond growth, debond length (d) is set equal to length of porous flow regime (x_0), where "A" is the projected area of debond, and p is partial pressure of oxygen inside the debond. From Darcy's law of flow in a porous medium, the rate of oxygen flow, u, into the debond region can be written, as given by Williams [14],

$$\frac{dx_0}{dt} = u = \frac{A}{c\eta}\left(\frac{dp}{dx}\right) \tag{8}$$

where η is the viscosity and c is a constant. Using Henry's Law, we can define a relation between pressure (p), and concentration of oxygen (C), inside the debond,

$$\text{Pressure } (p) = \text{Concentration } (C) * \text{Solubility } (S)$$

Substituting for pressure in Eq. 8, and assuming solubility is a constant, the modified form of Darcy's equation in terms of oxygen concentration (C) becomes,

$$\frac{dx_0}{dt} = u = \frac{SA}{c\eta}\left(\frac{dC}{dx}\right) \tag{9}$$

In the interest of tractability, assuming that oxygen diffusion inside the porous debond is incompressible, the continuity condition can be written as,

$$\frac{du}{dx} + \frac{dv}{dx} = 0 \tag{10}$$

where u and v represent velocity of oxygen flow in the x and y directions, respectively.

For a steady rate of diffusion in transverse direction, $dv/dx = 0$, giving,

$$\frac{du}{dx} = 0$$

Substituting this result in Eq. 9 gives,

$$\frac{d^2C}{dx^2} = 0 \tag{11}$$

or,

$$C = mx + b$$

The concentration boundary conditions are,

At $x = 0, C = C_0$ (oxygen concentration at the free edge)

or,

$$b = C_0$$

At $x = x_0$, $C = 0$, assuming zero oxygen concentration at the debond tip where void nucleation is taking place, giving,

$$m = \frac{-C_0}{x_0}$$

Therefore,

$$C = C_0\left(1 - \frac{x}{x_0}\right) \tag{12}$$

Combining (9) and (12) gives,

$$\frac{dx_0}{dt} = u = \frac{SA}{c\eta}\left(\frac{-C_0}{x_0}\right)$$

Integrating,

$$\int_0^d x_0 dx_0 = -\int_0^t \frac{SA}{c\eta} C_0 dt$$

or,

$$\frac{d^2}{2} = -\frac{SA}{c\eta} C_0 t$$

or,

$$d = \left(\frac{-2SAC_0}{c\eta}\right)^{1/2} \sqrt{t} \tag{13}$$

where "d" is the debond length. As evident from Eq. 13, for permeation-controlled debond growth, debond length at the fiber/matrix interface due to oxidative degradation is directly proportional to the square-root of time.

Least-squares fit for debond length from experiments

A least-squares fit was employed to fit the experimental data for debond length due to diffusion complying with square-root of time as shown in Fig. 4 for oxidation of a G30-500/PMR-15 unidirectional laminate in air at 288 °C.

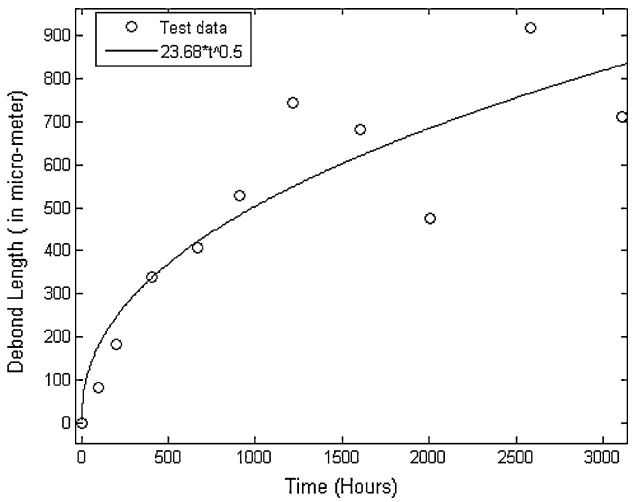

Fig. 4 Least squares curve fit for debond length versus time, of the form $B\sqrt{t}$

From the least-square fit, the following relationship between debond length d, and time, t was established,

$$d(t) = B\sqrt{t} \tag{14}$$

where $B = 23.68$ for G30-500/PMR-15. A comparison of the functional form of Eq. 14 with Eq. 13 corroborates the use of Darcy's law for predicting debond length due to permeation-controlled debond growth at the micro-scale. Oxygen concentration boundary conditions along the length of the debond given by Eq. 12, in conjunction with the diffusion-reaction equation for the polymer matrix (Eq. 1) and cohesive layer element at the fiber/matrix interface were incorporated in a in-house test-bed finite element code (NOVA-3D) to predict debond length as a function of time using a nonlinear finite element solution technique that takes into account the moving boundary at the debond tip. The material parameters used in the simulation are listed in Table 1. Figure 5 shows

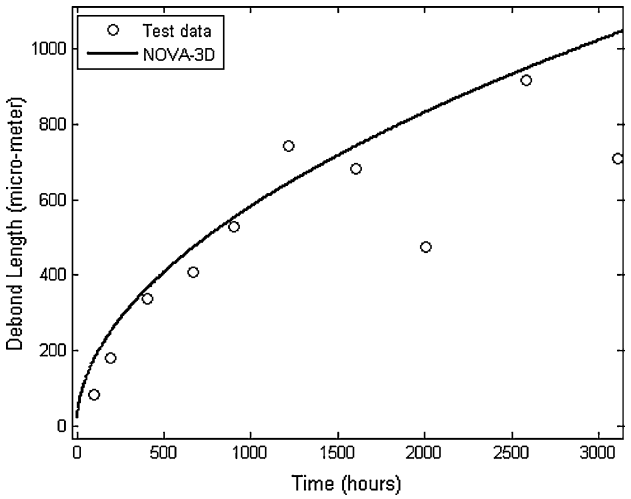

Fig. 5 Predicted debond length versus time from FEA analysis (NOVA-3D)

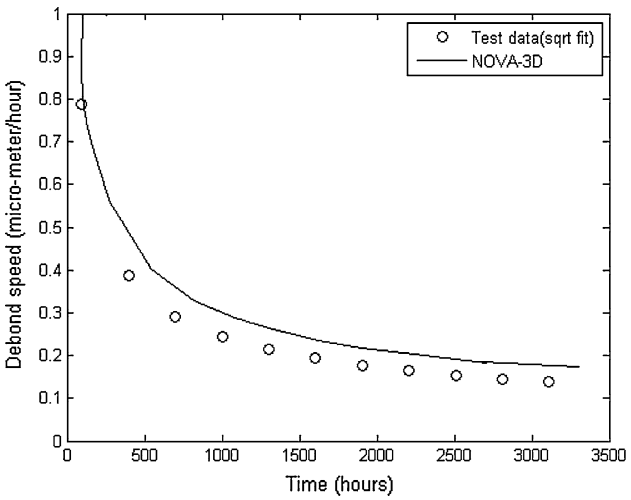

Fig. 6 Debond growth rate versus time using FEA for 5% shrinkage strain

that the debond length history predicted by NOVA-3D compares well with the evolution of average debond length from experimental data for G30-500/PMR-15, despite some scatter in the test data at higher aging times. In Fig. 6, debond growth rate computed from NOVA-3D is compared with least-squares fit of experimental data, again showing excellent agreement. As can be observed from this figure, after debond initiation at fiber/matrix interface near the laminate edge, the initial decrease in debond growth rate is very rapid. Subsequently, the debond growth rate asymptotically approaches a constant value after over 3000 h of exposure.

Anisotropic damage modeling for fiber/matrix debonding

Derivation of damage mechanics model

Based on the CDM approach proposed by Talreja [7, 8], Figure 7 shows a RVE with full circumferential fiber/matrix debond of length d. We assume that the debond surfaces are symmetric about three orthogonal planes, one of which splits a fiber longitudinally in two halves and the other is normal to the fiber axis. Assuming that the undamaged composite is transversely isotropic with the plane normal to the fiber axis as the plane of isotropy, we define the coordinate axes with X_1-axis parallel to fibers as shown in Fig. 7. For an RVE where V_f is fiber volume fraction, R is the fiber radius, L_R is the length of RVE, $d(t)$ is the fiber/matrix debond length in longitudinal direction at time t, and a is a damage influence parameter analogous to mode I crack-opening displacement, a symmetric damage tensor at the debond surface may be defined as [7],

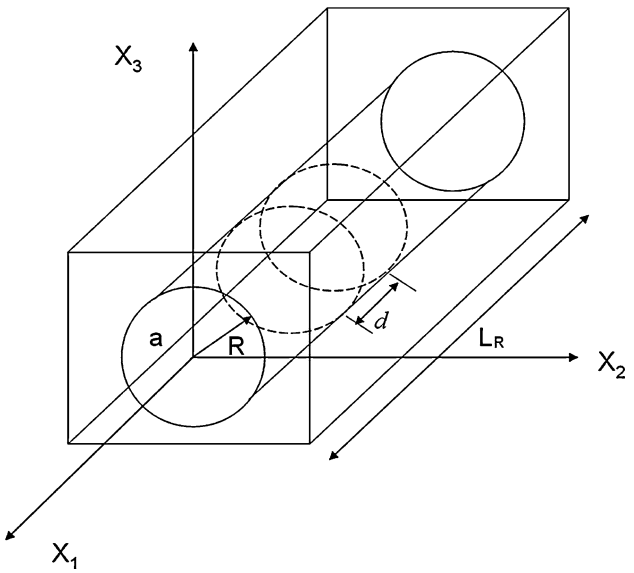

Fig. 7 Representative volume element containing fiber/matrix debond

$$d_{ij} = \frac{1}{V_{\mathrm{RVE}}} \int_S a n_i n_j \mathrm{d}S \tag{15}$$

where S is the area of the debond surface within the RVE, and the unit normal vector to the debond surface is given by,

$$\vec{n} = \pm \cos\theta\, \hat{e}_2 \pm \sin\theta\, \hat{e}_3 \tag{16}$$

with scalar components $n_1 = 0, n_2 = \mathrm{Cos}\ \theta$, and $n_3 = \mathrm{Sin}\ \theta$. The volume of the RVE is given by,

$$V_{\mathrm{RVE}} = \frac{\pi R^2 L_R}{V_f} \tag{17}$$

Because the component of the unit normal in the longitudinal direction is zero ($n_1 = 0$) at the debond surface, the component of the damage tensor in the longitudinal (fiber) direction is also zero, i.e., $d_{11} = 0$.

By substituting Eqs. (16) and (17) in Eq. (15), the component of the damage tensor normal to the debond surface in the X_2-direction at time t, is given by,

$$d_{22}(t) = \frac{1}{V_{\mathrm{RVE}}} \left(2 \int_0^{\pi} a \mathrm{Cos}^2\theta\, d(t)\, R \mathrm{d}\theta \right)$$

or,

$$d_{22}(t) = \frac{a V_f d(t)}{R L_R} = \delta(t) \tag{18}$$

Similarly, it can be shown that the component of the damage in the X_3-direction at time t is,

$$d_{33}(t) = \frac{1}{V_{\mathrm{RVE}}} \left(2 \int_0^{\pi} a \mathrm{Sin}^2\theta d(t) R \mathrm{d}\theta \right) = \frac{a V_f d(t)}{R L_R} \tag{19}$$

It is evident from Eqs. 18 and 19 that $d_{22} = d_{33} = \delta(t)$, and that d_{22} and d_{33} represent the same damage entity for a full circumferentially debonded fiber. If the crack opening displacement a is assumed to be proportional to a characteristic crack dimension [7], i.e., $a = k\sqrt{S}$, where S is the surface area of the debond, and k is a proportionality constant, then the damage parameter can be written as,

$$\delta(t) = \frac{k V_f d(t) \sqrt{S(t)}}{R L_R} \tag{20}$$

Defining $S(t) = 2\pi R d(t)$ as the area of debond at time t, the damage parameter can be expressed as,

$$\delta(t) = k V_f \sqrt{2\pi \left(\frac{L_R}{R}\right)} \left(\frac{d(t)}{L_R}\right)^{3/2} \tag{21}$$

Formulation of stiffness coefficient matrix for fiber/matrix debond

Thermo-mechanical response of a structure with internal damage can be described using fundamental principles

of irreversible thermodynamics [15]. The internal variable for the debond damage configuration is $\delta(t)$ as given by Eq. 21, and the response function has following form,

$$\Phi = \Phi(\varepsilon_{ij}, \delta) \tag{22}$$

The elements of integrity basis for transversely isotropic symmetry [16], retaining up to second-order term in ε_{ij} and linear terms in δ, assuming $\delta \ll 1$, are,

$$\begin{aligned}&\varepsilon_{11}, \varepsilon_{22}+\varepsilon_{33}, (\varepsilon_{22}-\varepsilon_{33})^2+4\varepsilon_{23}^2, \varepsilon_{12}^2\\&\quad+\varepsilon_{13}^2, \delta, \delta(\varepsilon_{22}-\varepsilon_{33}), \delta\varepsilon_{23}, \delta\varepsilon_{12}\varepsilon_{13}, \delta(\varepsilon_{12}^2-\varepsilon_{13}^2)\end{aligned} \tag{23}$$

The polynomial expansion of the Helmholz free energy function, Φ, in the absence of residual stresses, takes the following form [7],

$$\rho\Phi = \rho\Phi_0 + \rho\Phi_{\mathrm{d}} \tag{24}$$

where ρ is the density of the material, Φ_0 is a homogenously quadratic function of strain (ε_{ij}) representing the undamaged state of the material, and Φ_{d} is a homogeneously quadratic function of strain and a linear function of the damage parameter δ, incorporating the influence of damage on material stiffness. Constructed using the irreducible integrity bases given in Eq. 23, Φ_{d} has the following form [7],

$$\begin{aligned}\rho\Phi_{\mathrm{d}} &= A_1\delta\varepsilon_{11}^2 + A_2\delta(\varepsilon_{22}+\varepsilon_{33})^2 + A_3\delta\varepsilon_{11}(\varepsilon_{22}+\varepsilon_{33})\\&\quad+A_4\delta[(\varepsilon_{22}-\varepsilon_{33})^2+4\varepsilon_{23}^2]+A_5\delta(\varepsilon_{12}^2+\varepsilon_{13}^2)\\&\quad+A_6\delta(\varepsilon_{12}^2-\varepsilon_{13}^2)+A_7\delta\varepsilon_{12}\varepsilon_{13}+A_8\delta\varepsilon_{11}\varepsilon_{23}\\&\quad+A_9\delta\varepsilon_{23}(\varepsilon_{22}+\varepsilon_{33})+A_{10}\delta\varepsilon_{11}(\varepsilon_{22}-\varepsilon_{33})\\&\quad+A_{11}\delta(\varepsilon_{22}^2-\varepsilon_{33}^2)\end{aligned} \tag{25}$$

where A_1 through A_{11} are constant coefficients. The fourth-rank material stiffness tensor is given by the sum of the undamaged and damaged components,

$$C_{ijkl} = C^0_{ijkl} + C^d_{ijkl} \tag{26}$$

where

$$C^0_{ijkl} = \rho\frac{\partial^2\Phi_0}{\partial\varepsilon_{ij}\partial\varepsilon_{kl}} \quad \text{and} \quad C^d_{ijkl} = \rho\frac{\partial^2\Phi_d}{\partial\varepsilon_{ij}\partial\varepsilon_{kl}} \tag{27}$$

Here, C^0 is the stiffness tensor for an undamaged orthotropic elastic material, and the tensor C^d represents the change in stiffness coefficients due to the presence of damage in the form of fiber/matrix debonding.

Degradation of engineering moduli

Linearization of Eq. 27 leads to expressions for the in-plane engineering moduli after thermo-oxidative debonding damage has taken place, given by [7],

$$\begin{aligned}E_1^*(t) &= E_1^0 + 2\delta(t)[\bar{A}_1 - \bar{A}_2\nu_{12}^0 + \bar{A}_3(\nu_{12}^0)^2]\\E_2^*(t) &= E_2^0 + 2\delta(t)[\bar{A}_3 - \bar{A}_2\nu_{21}^0 + \bar{A}_1(\nu_{21}^0)^2]\\\nu_{12}^*(t) &= \nu_{12}^0 + 2\delta(t)\frac{1-\nu_{12}^0\nu_{21}^0}{E_2^0}\left[\frac{1}{2}\bar{A}_2 - \bar{A}_3\nu_{12}^0\right]\\G_{12}^*(t) &= G_{12}^0 + 2\delta(t)\bar{A}_2/4\end{aligned} \tag{28}$$

where E_1^0, E_2^0, ν_{12}^0, and G_{12}^0 are the in-plane elastic properties of the undamaged composite lamina, and $\bar{A}_1$, $\bar{A}_2$, $\bar{A}_3$ and $\bar{A}_4$ are constant coefficients from the CDM model. A numerical methodology for determining the unknown constant coefficients is presented in next section.

Evaluation of continuum damage mechanics coefficients

Three-dimensional finite element simulations [17], with a cohesive layer at fiber/matrix interface, were performed to obtain the damage mechanics coefficients defined in the previous section. The following load cases were simulated applying iso-strain boundary conditions to the RVE depicted in Fig. 7:

1. Axial tension (applied normal strain ε_{11} = constant, $\varepsilon_{22} = 0$, $\varepsilon_{33} = 0$)
2. Transverse tension (applied normal strain ε_{22} = constant, $\varepsilon_{11} = 0$, $\varepsilon_{33} = 0$)
3. Axial tension with Poisson effect (applied normal strain ε_{11} = constant, $\varepsilon_{33} = 0$, $\varepsilon_{22} = 0$ is unconstrained)
4. In-plane-shear (applied shear strain γ_{12} = constant)

The FEA simulations were post-processed to obtain the total strain-energy for the RVE for each of the above reference cases, for a specified debond length, δ. Using energy equivalence between the micromechanical RVE and a smeared orthotropic continuum model of the RVE, the unknown CDM coefficients $\bar{A}_1, \bar{A}_2, \bar{A}_3$, and $\bar{A}_4$ were obtained by employing a least-squares fit. The CDM coefficients thus obtained are tabulated in Table 2. Having determined the CDM coefficients, the damaged orthotropic lamina properties E_{11}^*, E_{22}^*, ν_{12}^*, and G_{12}^*, were then obtained as a function of debond length as defined in Eq. 28. The fiber volume fraction for the FEA simulation was assumed to be 0.6. The fiber and matrix properties for G30-500/PMR-15 composite used in these simulations are given in Table 1.

Damage evolution model for a composite laminate

Consider a unidirectional G30-500/PMR-15 laminate of thickness h, subjected to a load P at the mid-span as shown in Fig. 8. In this case study, the unidirectional fibers are assumed to run parallel to the X-axis, and thermo-oxidative

Table 2 Coefficients of CDM for $V_f = 0.6$

CDM coefficients	Values
A_1 (MPa)	-3.981×10^3
A_2 (MPa)	-10.424×10^3
A_3 (MPa)	-1.513×10^3
A_4 (MPa)	-1.67×10^3
k	0.02–0.05

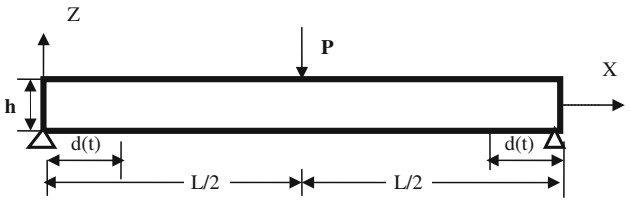

Fig. 8 Thermo-oxidative degradation of symmetric unidirectional laminate under three-point bending load

degradation of the laminate is assumed to occur primarily due to the progressive debonding of the fiber/matrix interface at the free edges of the laminate induced by shrinkage stresses in the matrix due to oxidation. Assume that the average extent of the zone of thermal-oxidative degradation from the laminate edge at time t is given by $d(t)$, as shown in Fig. 8. For an orthotropic unidirectional symmetric laminate undergoing cylindrical bending, the moment curvature relationship reduces to,

$$D_{11}^{*}\frac{d^2w^{*}}{dx^2} = M(x) \quad 0<x<d(t) \tag{29}$$

where the bending stiffness after thermo-oxidative damage,

$$D_{11}^{*} = \frac{1}{12}bh^3\left(\frac{E_1^{*}}{1-v_{12}^{*}v_{21}^{*}}\right) \tag{30}$$

In Eqs. 29 and 30, b is the width of the laminate, h is the thickness, and $M(x)$ is the applied bending moment. Superscript (*) denotes material properties that have undergone thermo-oxidative damage, as defined in Eq. 28. Assuming that the average length of the interfacial debond is $d(t)$ at time t, and using symmetry, the moment–curvature relationship for the undamaged laminate can be expressed as,

$$D_{11}\frac{\mathrm{d}^2w}{\mathrm{d}x^2} = M(x) \quad d(t)<x<L/2 \tag{31}$$

where,

$$D_{11} = \frac{1}{12}bh^3\left(\frac{E_1^{0}}{1-v_{12}^{0}v_{21}^{0}}\right) \tag{32}$$

For three-point bending of a simply supported laminate as shown in Fig. 8, the bending moment is,

$$M(x) = -\frac{P}{2}x \quad 0<x<L/2 \tag{33}$$

For the debonded portion of the laminate at time t, substituting (33) in (29),

$$D_{11}^{*}\frac{\mathrm{d}^2w^{*}}{\mathrm{d}x^2} = -\frac{P}{2}x$$

$$\frac{\mathrm{d}w^{*}}{\mathrm{d}x} = -\frac{P}{4D_{11}^{*}}x^2 + c_1 \tag{34}$$

$$w^{*}(x) = -\frac{P}{12D_{11}^{*}}x^3 + c_1x + c_2 \tag{35}$$

Applying boundary condition, that at $x = 0$, $w(0) = 0$, gives,

$$w^{*}(0) = c_2 = 0 \tag{36}$$

Substituting (36) in (35) gives,

$$w^{*}(x) = -\frac{P}{12D_{11}^{*}}x^3 + c_1x \quad 0<x<d(t) \tag{37}$$

For the undamaged portion of the laminate at time t, substituting (33) in (31),

$$\frac{\mathrm{d}^2w}{\mathrm{d}x^2} = -\frac{Px}{2D_{11}}$$

$$\frac{\mathrm{d}w}{\mathrm{d}x} = -\frac{Px^2}{4D_{11}} + c_3 \tag{38}$$

$$w(x) = -\frac{Px^3}{12D_{11}} + c_3x + c_4 \tag{39}$$

Applying symmetry boundary condition that at $x = L/2$, $\mathrm{d}w/\mathrm{d}x = 0$, gives,

$$\left.\frac{\mathrm{d}w}{\mathrm{d}x}\right|_{x=\frac{L}{2}} = -\frac{P}{4D_{11}}\left(\frac{L^2}{4}\right) + c_3 = 0$$

or,

$$c_3 = \frac{PL^2}{16D_{11}} \tag{40}$$

Therefore,

$$w(x) = -\frac{Px^3}{12D_{11}} + \frac{PL^2x}{16D_{11}} + c_4 \tag{41}$$

Enforcing continuity of deflection and slope at the point where the damaged and the undamaged laminate meet, i.e., at $x = d(t)$,

$$w^{*}(d(t)) = w(d(t)) \tag{42}$$

$$\left.\frac{\mathrm{d}w^{*}}{\mathrm{d}x}\right|_{x=d(t)} = \left.\frac{\mathrm{d}w}{\mathrm{d}x}\right|_{x=d(t)} \tag{43}$$

Enforcing Eq. 43, combining Eqs. (34), (38), and (40),

$$c_1 = \frac{PL^2}{16D_{11}} + \frac{Pd^2(t)}{4}\left(\frac{1}{D_{11}^*} - \frac{1}{D_{11}}\right) \tag{44}$$

Enforcing Eq. 42, combining Eqs. 37 and 41,

$$c_4 = \frac{Pd^3(t)}{12}\left(\frac{1}{D_{11}} - \frac{1}{D_{11}^*}\right) - \frac{PL^2 d(t)}{16D_{11}} + c_1 d(t) \tag{45}$$

Finally, an expression for the deflection at the mid-span of the thermo-oxidatively aged laminate can be obtained by combining Eqs. 41, 44, and 45,

$$w\left(\frac{L}{2}\right)_{\text{aged}} = \frac{PL^3}{48D_{11}} - \frac{Pd^3(t)}{6}\left(\frac{1}{D_{11}} - \frac{1}{D_{11}^*}\right) \tag{46}$$

As a baseline for comparison, the deflection at the mid-span of an equivalent unaged (undamaged) laminate of length L due to three point bending is given by,

$$w\left(\frac{L}{2}\right)_{\text{unaged}} = \frac{PL^3}{48D_{11}} \tag{47}$$

It is evident that Eq. 46 reduces to Eq. 47 when debond damage length $d(t)$ is zero, in which event $D_{11}^* = D_{11}$.

If we rewrite Eq. 46 in the form,

$$w\left(\frac{L}{2}\right)_{\text{aged}} = \frac{PL^3}{48\overline{D}_{11}}$$

where $\bar{D}_{11}$ is the overall effective (damaged) laminate bending stiffness, then,

$$\overline{D}_{11}(d(t)) = \frac{PL^3}{48w\left(\frac{L}{2}\right)_{\text{aged}}} \tag{48}$$

where $w(L/2)$ is given by Eq. 46.

Finally, the normalized effective bending stiffness for the aged laminate can be obtained from Eqs. 48, 46, and 32,

$$\frac{\overline{D}_{11}}{D_{11}} = \frac{PL^3}{48D_{11}w\left(\frac{L}{2}\right)_{\text{aged}}} \tag{49}$$

Results and discussion

In the laminate analysis results presented in this section, the evolution of the average fiber/matrix debond length, $d(t)$, as a function of time is obtained using Eq. 14. The corresponding damage parameter $\delta(t)$ for the laminate analysis is defined by setting the debond length equal to the micromechanical RVE length (i.e., $d(t) = L_R$) in Eq. 21, representing a fully debonded fiber/matrix interface of length $d(t)$ at time t, giving,

$$\delta(t) = kV_f\sqrt{2\pi\left(\frac{d(t)}{R}\right)} \tag{50}$$

The predicted variation of normalized bending stiffness ($\bar{D}_{11}/D_{11}$) with normalized fiber/matrix debond length for a unidirectional G30-500/PMR-15 laminate is shown in Fig. 9 for different values of the damage opening proportionality constant k (refer to Eq. 20). Figure 10 depicts the predicted variation of normalized laminate bending stiffness ($\bar{D}_{11}/D_{11}$) with time, based on the NOVA-3D predictions of the debond growth rate shown in Fig. 5. From these figures, it is evident that, initially, the effect of debond growth on bending stiffness is not very significant until the debond length, $d(t)$, from each edge approaches $\sim$15% of the laminate span. Subsequently, a dramatic reduction in the effective bending stiffness is predicted as the debond length increases with time. A parametric sensitivity study of the influence of the damage opening proportionality constant k on effective bending stiffness as depicted in Figs. 9 and 10 reveals that the effective bending

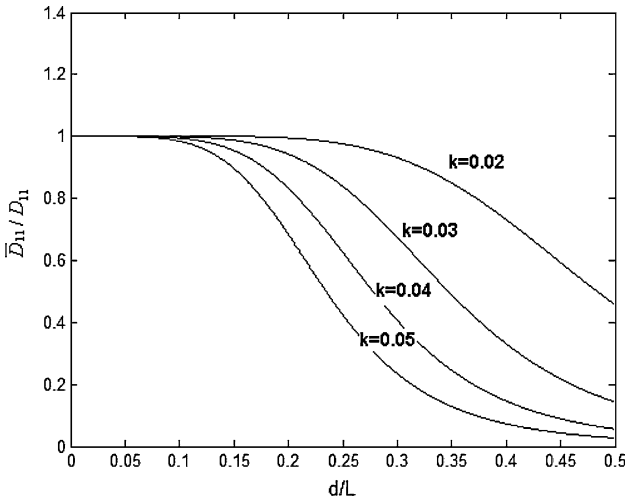

Fig. 9 Variation of normalized bending stiffness $\bar{D}_{11}/D_{11}$ with debond length for different values of the damage parameter k

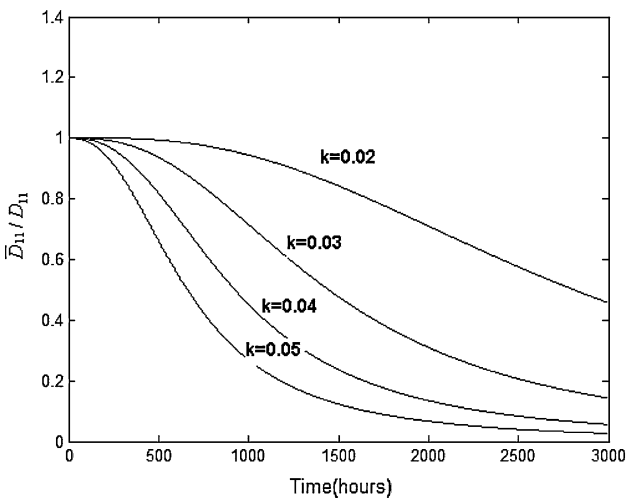

Fig. 10 Variation of normalized bending stiffness $\bar{D}_{11}/D_{11}$ with time for different values of the damage parameter k

stiffness is quite sensitive to the value of k for the range of properties selected in the present analysis.

Conclusions

In this paper, a simple methodology is presented for transitioning from a micro-mechanics (RVE)-based kinetic model to the macro-scale structural level, through the use of CDM. The strong anisotropy in the longitudinal direction observed in the thermal-oxidation of unidirectional composite lamina is accounted for in this model. Darcy's law is employed to model oxygen permeation in the porous region at the fiber/matrix interface to develop a shrinkage-induced permeation-controlled debond growth model. Debond initiation and growth is incorporated in the model through the use of a cohesive layer with a prescribed traction-separation law, and the damage parameters thus obtained are used to predict long-term behavior at the laminate level.

From the analytical predictions it is evident that, initially, the effect of debond growth on laminate bending stiffness is not very significant until the debond length, $d(t)$, from each edge approaches $\sim 15\%$ of the laminate span. Subsequently, a dramatic reduction in the effective bending stiffness is predicted as the debond length increases with time. A parametric sensitivity study of the influence of the damage opening proportionality constant k on effective bending stiffness reveals that the effective bending stiffness is quite sensitive to the value k for the range of properties selected in the present analysis.

It should be noted that the influence of temperature on the CDM parameters is not included in this analysis due to a lack of characterization data. Further, fiber/matrix debond is considered as the principal damage mode because there is little evidence that other damage modes, such as transverse matrix cracking, significantly influences laminate bending stiffness for the composite under consideration. It should also be noted that the CDM-based analytical model for predicting laminate stiffness degradation as presented in the previous section is valid only for unidirectional laminates undergoing three-point bending, and for a square packing of the micromechanical RVE. However, the same multi-scale modeling methodology presented in this paper can be readily implemented in a three-dimensional finite element code to predict changes in stiffness due to thermo-oxidative degradation in composite laminates with arbitrary ply orientation subjected to complex load histories. Work is currently underway to implement the multi-scale CDM model in a three-dimensional finite element code.

Acknowledgements The authors gratefully acknowledge the support of the Mechanics of Multifunctional Materials & Microsystems Program of the Air Force Office of Scientific Research, with Dr. Byung "Les" Lee as Program Manager.

References

1. Colin X, Verdu J (2005) Compos Sci Technol 65:411. doi:10.1016/j.compscitech.2004.09.011
2. Colin X, Marais C, Verdu J (2005) Compos Sci Technol 65:117. doi:10.1016/j.compscitech.2004.06.009
3. Tandon GP, Pochiraju KV, Schoeppner GA (2006) Polym Degrad Stab 91(8):1861. doi:10.1016/j.polymdegradstab.2005.11.008
4. Pochiraju KV, Tandon GP (2006) J Eng Mater Technol 128:107. doi:10.1115/1.2128427
5. Pochiraju KV, Tandon GP, Schoeppner GA (2008) Mech Time-Depend Mater 12:45. doi:10.1007/s11043-007-9042-5
6. Wang SS, Chen X (2006) J Eng Mater Technol 128:81. doi:10.1115/1.2132377
7. Talreja R (1991) Mech Mater 12:165. doi:10.1016/0167-6636(91)90061-4
8. Talreja R (2006) J Mater Sci 41:6800. doi:10.1007/s10853-006-0210-9
9. Crank J (1975) Mathematics of diffusion, 2nd edn. Clarendon Press, Oxford
10. Roy S, Wang Y, Park S, Liechti KM (2006) ASME J Eng Mater Technol 128(1):11. doi:10.1115/1.2127959
11. Roy S, Wang Y, Park S, Xu D, Liechti KM (2007) J Mech Adv Mater Struct 14:1. doi:10.1080/15376490600985227
12. Needleman A (1987) J Appl Mech 54:525
13. Wise J, Gillen KT, Clough RL (1997) Polymer 38:1929. doi:10.1016/S0032-3861(96)00716-1
14. Williams JG (1984) Fracture mechanics of polymers. Ellis Horwood Limited
15. Coleman BD, Gurtin ME (1967) J Chem Phys 47:597
16. Smith GF (1982) Quart Appl Math 39:509
17. ABAQUS, Version 6.5 (2004) *Hibbit, Karlsson, and Sorensen Inc.,* Providence, Rhode Island